

# 1 **Cortical areas for planning sequences before and during movement**

2 Giacomo Ariani<sup>1,2,†</sup>, Mahdiyar Shahbazi<sup>1,†</sup>, Jörn Diedrichsen<sup>1,2,3,\*</sup>

3  
4 <sup>1</sup>Western Institute for Neuroscience, <sup>2</sup>Department of Computer Science, <sup>3</sup>Department of Statistical and Actuarial Sciences, Western  
5 University, London, ON N6A3K7, Canada.

6  
7 †These authors contributed equally to this work

8 \*Correspondence should be addressed to Jörn Diedrichsen at [jdiedric@uwo.ca](mailto:jdiedric@uwo.ca)

9  
10 **Abbreviated title.** Planning sequences before and during movement

11  
12 Number of pages: 24

13 Number of figures: 4

14 Number of tables: 1

15 Number of words for abstract: 201 / 250

16 Number of words for introduction: 573 / 650

17 Number of words for discussion: 965 / 1500

18  
19 **Author contributions.** G.A. and J.D. designed research; G.A. performed research; M.S. and G.A. analyzed data;  
20 All authors drafted and edited the manuscript.

21  
22 **Acknowledgments.** This work was supported by a Discovery Grant from the Natural Sciences and Engineering  
23 Research Council of Canada (NSERC, RGPIN-2016-04890) and a project grant from the Canadian Institutes of  
24 Health Research (CIHR, PJT-175010) to J.D., and the Canada First Research Excellence Fund (BrainsCAN).

25  
26 **Disclosures.** The authors declare no conflicts of interest.

## 28 **Abstract**

29 Production of rapid movement sequences relies on preparation before (pre-planning) and during (online planning)  
30 movement. Here, we asked how different cortical sensorimotor areas contribute to these processes. Human  
31 participants performed three single-finger and three multi-finger sequences in a delayed movement paradigm.  
32 During preparation, 7T functional MRI revealed that primary motor (M1) and somatosensory (S1) areas showed  
33 pre-activation of the first movement, even though the overall activation level did not change from baseline. During  
34 production, the activity in M1 and S1 could be explained by temporal summation of activity patterns  
35 corresponding to constituent fingers. In contrast, dorsal premotor (PMd) and anterior superior parietal lobule  
36 (aSPL) showed substantial activation during preparation of multi-finger as compared to single-finger sequences.  
37 The same regions were also more activated during production of multi-finger sequences, suggesting that the same  
38 areas are involved in both pre- and online planning. Nonetheless, we observed small but robust differences  
39 between the two contrasts, suggesting preferential involvements of these areas in pre- and online planning.  
40 Multivariate analysis revealed sequence-specific representations in both PMd and aSPL, which remained stable  
41 across both preparation and production phases. This suggests that these areas maintain a sequence-specific  
42 representation before and during sequence production, likely guiding the execution-related areas.

## 43 **Keywords**

44 Sequential movements; Motor planning; Hand control; fMRI; MVPA.

## 45 **Significance Statement (120 max)**

46 Understanding how the brain orchestrates complex behavior remains a core challenge in human neuroscience.  
47 Here, we combine high-resolution neuroimaging and a carefully crafted design to study the neural control of rapid  
48 sequential finger movements, like typing or playing the piano. Advancing prior research, we show that the brain  
49 areas involved in planning these movements maintain those representations throughout the execution of the  
50 sequence. This representational stability across planning and execution suggests an intricate connection between  
51 these processes. Our results shed light on the nuanced contributions of different cortical areas to different aspects  
52 of coordinating skilled movement. This work is well placed to inform future research in animal models and the  
53 development of targeted interventions against movement disorders.

## 54 **Introduction (650 max)**

55 From buttoning a shirt to texting with a smartphone, many everyday actions depend on the brain's ability to  
56 coordinate rapid sequences of finger movements. Behavioral studies have demonstrated that, when tasked to  
57 produce a sequence of multiple finger presses, participants pre-plan the first two or three elements before sequence  
58 production starts (Ariani & Diedrichsen, 2019; Ariani et al., 2021). Once the sequence starts, planning the  
59 upcoming movements continues throughout sequence production, a process called online planning. Most

60 behavioral improvements during motor sequence learning can be explained by participants becoming faster at  
61 pre- and online planning (Ariani & Diedrichsen, 2019). Which, and how, different cortical motor areas contribute  
62 to these different aspects of motor sequence planning, however, is poorly understood.

63 Previous neuroimaging studies of motor sequences have used multivariate analysis of fMRI data to reveal  
64 a hierarchy of sequence representations across cortical motor areas (Berlot et al., 2020; Yokoi et al., 2018; Yokoi  
65 & Diedrichsen, 2019). The dorsal premotor cortex (PMd) and the superior parietal lobule (SPL) exhibit sequence-  
66 specific representations, i.e., activity patterns that encode the specific sequence of actions, not just the individual  
67 movements themselves. Sequence-specific representations in association cortex have also been shown using  
68 electrophysiology in non-human primates (Russo et al., 2020; Shima et al., 2006; Tanji & Shima, 1994). In  
69 contrast, activity patterns in the primary motor (M1) and somatosensory cortex (S1) could be explained by a  
70 summation of the patterns related to the individual finger presses (Berlot et al., 2021; Yokoi et al., 2018). Due to  
71 difficulties related to fMRI temporal resolution, however, this work did not distinguish between activity arising  
72 from sequence planning or execution. Although Gallivan et al. (2016) showed that sequences of two upper-limb  
73 actions (e.g., reaching to grasp and place vs. hold a cup) could be distinguished from preparatory fMRI activity  
74 patterns, but the nature of these representations remains unknown.

75 Here, we used high-field (7T) fMRI while human participants planned and executed both multi- and  
76 single-finger sequences on a keyboard device (matched number of keypresses across sequences). A delayed-  
77 movement paradigm with no-go trials (Ariani et al., 2018) allowed us to isolate brain activity related to planning  
78 and execution and address the following three questions about the role of cortical areas in sequence planning.

79 First, we investigated brain responses in primary sensorimotor cortex (M1 and S1) during the preparation  
80 of a sequence. For single-finger actions, we have previously shown that movement planning pre-activates the  
81 relevant finger-specific activity pattern in both M1 and S1 (Ariani et al., 2022). But what is the preparatory state  
82 in M1 for multi-finger movements?

83 Second, recent behavioral studies suggest that online planning of movement sequences shares important  
84 behavioral features with sequence pre-planning—both exhibit a similar planning horizon and both contribute to  
85 performance improvements with sequence learning (Ariani & Diedrichsen, 2019; Ariani et al., 2021). We  
86 therefore tested to what degree pre- and online planning engage the same cortical areas by contrasting multi- and  
87 single-finger movements during preparation and production phases.

88 Finally, employed multi-variate analysis to study two of the identified brain regions, PMd and SPL, in  
89 more depth. Previous results (Berlot et al., 2021; Yokoi & Diedrichsen, 2019) have revealed sequence-specific  
90 representations in both. Our paradigm now allowed us to ask whether these representations are present only during  
91 preparation or whether they persist during movement production. Furthermore, we investigated to what degree  
92 the sequence-specific representations underlying pre- and online planning are the same, or whether they  
93 dynamically change from preparation to production.

## 94 **Materials and Methods**

### 95 *Participants*

96 Twenty-three right-handed neurologically healthy participants volunteered to take part in the experiment (13 F,  
97 10 M; age 20–31 years, mean 23.43 years, SD 4.08 years). Criteria for inclusion were right-handedness and no  
98 prior history of psychiatric or neurological disorders. Handedness was assessed with the Edinburgh Handedness  
99 Inventory (mean 82.83, SD 9.75). All experimental procedures were approved by the Research Ethics Committee  
100 at Western University. Participants provided written informed consent to procedures and data usage and received  
101 monetary compensation for their participation. One participant withdrew before study completion and was  
102 excluded from data analysis (final N = 22). A part of the data used in the current paper was previously published  
103 (Ariani et al., 2022).

### 104 *Apparatus*

105 Sequences of right-hand finger presses were performed on a custom-made MRI-compatible keyboard device (Fig.  
106 1A). Participants used their fingers to press the keys. The keys of the device did not move, but force transducers  
107 underneath each key measured isometric force production at an update rate of 2 ms (Honeywell FS series;  
108 dynamic range 0-25 N). A keypress/release was detected when the force crossed a threshold of 1 N. The forces  
109 measured from the keyboard were low pass filtered to reduce noise induced by the MRI environment, amplified,  
110 and sent to the PC for online task control and data recording.

### 111 *Task*

112 We used a task in which participants produced sequences of keypresses with their right-hand fingers in response  
113 to numerical cues (Fig. 1B) presented on a computer screen that was visible to the participants lying in the scanner  
114 through an angled mirror. On each trial, a string of 6 numbers (instructing cue) instructed which sequence to plan  
115 (Fig. 1C, white outline).

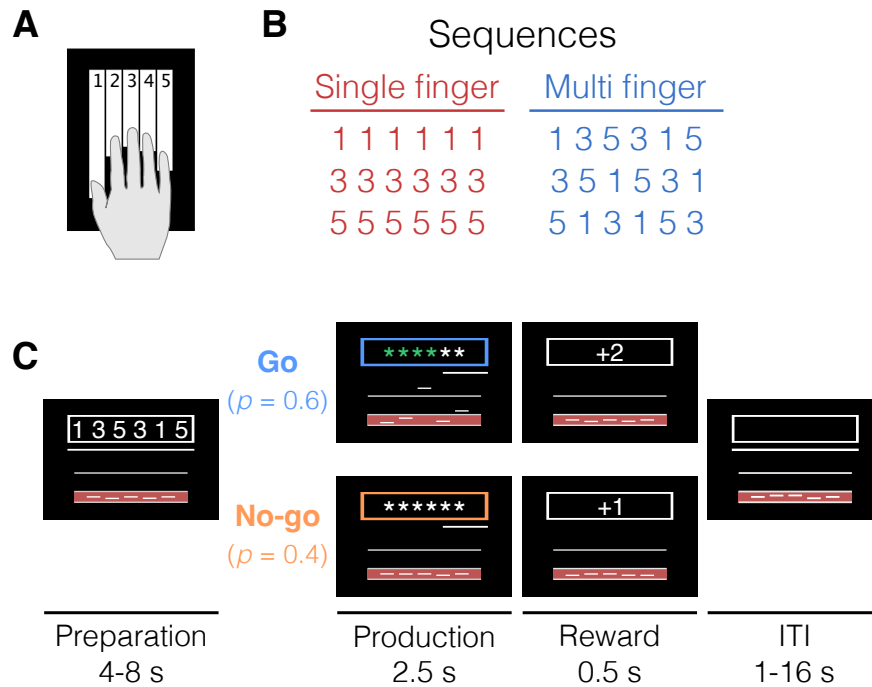


**Figure 1. Sequence conditions and task timing.** (A) Response keyboard with mapping between numbers and fingers. Numbers were not visible on the keys. (B) Digits presented on the screen for single-finger (red) and multi-finger sequences (blue). (C) Temporal structure of a trial. During the preparation phase, a sequence of 6 numbers was displayed within a box at the top of the screen. With a probability of 0.6, the box frame then changed to a blue color, instructing participants ( $N=22$ ) to produce the memorized sequence as fast as possible (go trials). Each correct press caused an asterisk to turn green. With 0.4 probability, the box frame turned orange, signaling participants to withhold the response (no-go trials). ITI = inter-trial interval.

The length of the preparation phase was randomly sampled to be 4 s (56% of trials), 6 s (30%), or 8 s (14%). To control for involuntary overt movements during the preparation phase, we required participants to maintain a steady force of around 0.25 N on all the keys during the delay, which was closely monitored online. As a visual aid, we displayed a red area (between 0 and 0.5 N) and asked participants to remain in the middle of that range with all the fingers (touching either boundary of the red area would count as unwanted movement, thus incurring an error).

At the onset of the production phase, participants received a color cue (go/no-go cue) indicating whether to perform the planned finger presses (blue outline = go,  $p = 0.6$ ) or not (orange outline = no-go,  $p = 0.4$ ). The role of no-go trials was to dissociate the hemodynamic response to the successive preparation and production events, which would otherwise always overlap in fast fMRI designs due to the sluggishness of the fMRI response. To encourage planning during the delay period, at the go cue, the digits were masked with asterisks at go-cue onset, and participants had to perform the presses from memory. Participants had 2.5 s to complete the sequence of 6 presses, and a vanishing white bar under the asterisks indicated how much time was left. Participants received online feedback on the correctness of each press with asterisks turning either green, for a correct press or red, for

incorrect presses. As long as the participants remained within task constraints (i.e., 6 keypresses in less than 2.5 s), an exact movement speed was not enforced. In no-go trials, participants were instructed to remain as still as possible, maintaining the finger pre-activation until the end of the production phase (i.e., releasing any of the keys would incur an error).

During the reward phase (0.5 s), points were awarded based on performance and according to the following scheme: -1 point in case of no-go error or go cue anticipation (timing errors); 0 points for pressing any wrong key (press error); 1 point in case of a correct no-go trial; and 2 points in case of a correct go trial. Inter-trial-intervals (ITI, gray background) were randomly drawn from {1, 2, 4, 8, 16 s} with the respective proportion of trials {52%, 26%, 13%, 6%, 3%}.

### ***Experimental design and structure***

Our chosen distribution of preparation times, inter-trial intervals, and no-go trials were determined by minimizing the variance inflation factor (VIF). VIF is the ratio of the mean estimation variance of all regression weights (preparation- and production-related regressors for each sequence) to the mean estimation variance had these regressors been estimated in isolation. Therefore, VIF quantifies the severity of multicollinearity between model regressors by providing an index of how much the variance of an estimated regression coefficient is increased because of collinearity. Large values for VIF mean that model regressors are not independent of each other, whereas a VIF of 1 means no inflation of variance. After optimizing the design, VIF was on average 1.15, indicating that we could separate planning and execution-related activity without a large loss of experimental power.

Participants underwent one fMRI session consisting of 10 functional runs and 1 anatomical scan. In an event-related design, we randomly interleaved 3 types of repeated single-finger presses involving the thumb (1), the middle (3), and the little (5) fingers (e.g., 111111 for thumb presses, Fig. 1B) and 3 types of multi-finger sequences (e.g., 135315). The day before the fMRI scan, participants familiarized themselves with the experimental apparatus and the go/no-go paradigm in a short behavioral session of practice outside the scanner (5 blocks, about 15-30 minutes in total). For the behavioral practice, inter-trial intervals were kept to a fixed 1 s to speed up the task, and participants were presented with different sequences from what they would see while in the scanner. These 6-item sequences were randomly selected from a pool of all possible permutations of the numbers 1, 3, and 5, with the exclusion of sequences that contained consecutive repetitions of the same number. Each sequence trial type (e.g., 111111) was repeated 5 times (2 no-go and 3 go trials), totaling 30 trials per functional run. Two periods of 10 seconds rest were added at the beginning and at the end of each functional run to allow for signal relaxation and provide a better estimate of baseline activation. Each functional run took about 5.5 minutes, and the entire scanning session (including the anatomical scan and setup time) lasted for about 75 minutes.

## 171 ***Imaging data acquisition***

172 High-field functional magnetic resonance imaging (fMRI) data were acquired on a 7T Siemens Magnetom  
173 scanner with a 32-channel head coil at Western University (London, Ontario, Canada). The anatomical T1-  
174 weighted scan of each participant was acquired halfway through the scanning session (after the first 5 functional  
175 runs) using a Magnetization-Prepared Rapid Gradient Echo sequence (MPRAGE) with a voxel size of  
176 0.75x0.75x0.75 mm isotropic (field of view = 208 x 157 x 110 mm, encoding direction coronal). To measure the  
177 blood-oxygen-level dependent (BOLD) responses in human participants, each functional scan (330 volumes) used  
178 the following sequence parameters: GRAPPA 3, multi-band acceleration factor 2, repetition time [TR] = 1.0 s,  
179 echo time [TE] = 20 ms, flip angle [FA] = 30 deg, slice number: 44, voxel size: 2x2x2 mm isotropic. To estimate  
180 and correct for magnetic field inhomogeneities, we also acquired a gradient echo field map with the following  
181 parameters: transversal orientation, a field of view: 210 x 210 x 160 mm, 64 slices, 2.5 mm thickness, TR = 475  
182 ms, TE = 4.08 ms, FA = 35 deg.

## 183 ***Preprocessing and univariate analysis***

184 Preprocessing of the functional data was performed using SPM12 ([fil.ion.ucl.ac.uk/spm](http://fil.ion.ucl.ac.uk/spm)) and custom MATLAB  
185 code. This included correction for geometric distortions using the gradient echo field map (Hutton et al., 2002),  
186 and motion realignment to the first scan in the first run (3 translations: x, y, z; 3 rotations: pitch, roll yaw). Due  
187 to the short TR, no slice timing corrections were applied. The functional data were co-registered to the anatomical  
188 scan, but no normalization to a standard template or smoothing was applied during preprocessing. To allow  
189 magnetization to reach equilibrium, the first four volumes of each functional run were discarded. The pre-  
190 processed images were analyzed with a general linear model (GLM). We defined separate regressors for each  
191 combination of the 6 finger-actions (single, multi) x 3 phases (preparation go, preparation no-go, production),  
192 resulting in a total of 18 regressors (12 go + 6 no-go), plus the intercept, for each run. We also conducted an  
193 analysis where the same preparation regressor was used in go and no-go, which resulted in qualitatively similar  
194 as reported here. For the main text, however, we decided to be conservative and not use the regressors for the  
195 preparation of go trials, thereby controlling for a residual bias from the execution-related activity onto the  
196 preceding planning-related activity. Each regressor consisted of boxcar functions of length 2s convolved with a  
197 two-gamma canonical hemodynamic response function with a peak onset at 5 s and a post-stimulus undershoot  
198 minimum at 10 s. Given the relatively low error rates (i.e., number of error trials over the total number of trials,  
199 timing errors:  $7.58 \pm 0.62$  %; press errors:  $1.18 \pm 0.26$  %; see Task above), all trials were included to estimate  
200 the regression coefficients, regardless of whether the execution was correct or erroneous. Ultimately, the first-  
201 level analysis resulted in activation images (beta maps) for each of the 18 conditions per run, for each of the  
202 participants.

## 203 ***Surface reconstruction***

204 Based on the 0.75mm anatomical scan, we reconstructed each individual cortical surface. Individual participants'  
205 cortical surfaces were reconstructed using Freesurfer (Dale et al., 1999). First, we extracted the white-gray matter  
206 and pial surfaces from each participant's anatomical image. Next, we inflated each surface into a sphere and  
207 aligned it using sulcal depth and curvature information to the Freesurfer average atlas (Fischl et al., 1999).  
208 Subsequently, surfaces were resampled to a left-right symmetric template (fs\_LR.164k.spec; Van Essen et al.,  
209 2012) included in the connectome workbench distribution (Marcus et al., 2011). The functional imaging data  
210 (2mm resolution) was then mapped onto this surface. In this analysis we excluded voxels that lay within the sulci  
211 and touch both banks (with more than 25% of the voxel volume in the grey matter on both sides sulcus). The  
212 individual surface maps were brought into alignment by morphing the surfaces based on the depth and curvature  
213 (van Essen et al., 2012). This approach is currently the state-of-the-art in imaging analysis to achieve the best  
214 regional specificity of group analysis despite the considerable inter-subject variability in cortical folding.

## 215 ***Regions of interest (ROI)***

216 We focused our imaging analysis on the dorsolateral aspect of the contralateral (left) hemisphere (purple area of  
217 Fig. 2A), including the motor regions of the medial wall.

218 To summarize the results and for statistical analysis, we have used a set of motor-related ROIs on the  
219 cortical surface that we have used consistently in previous papers (Ariani et al., 2022; Berlot et al., 2020, 2019;  
220 Jörn Diedrichsen et al., 2013; Yokoi et al., 2018). The definition relies on a post-mortem cytoarchitectonic  
221 analysis of 10 human brains (Fischl et al., 2008) that were normalized into a spherical (surface-based) group atlas.  
222 In comparison to a volume-based normalization of the same maps (Eickhoff et al., 2007), this approach leads to  
223 a cleaner separation of cortical areas. One of the limitations of such ROI-based approaches is potentially  
224 combining functional heterogeneous regions into a single ROI. For the current paper, we therefore chose a more  
225 refined approach that allows us to study differences in function within these ROIs in a more continuous manner,  
226 while still summarizing the data better than the map-wise approach.

227 For visualization of the functional profiles along the cortical surface, we defined an anterior-posterior line  
228 through the anatomically defined hand-knob (Yousry et al., 1997) that ran approximately orthogonal to the  
229 boundaries between different Brodmann areas (BA; Fischl et al., 2008). By extending the line  $\pm 20$  mm above and  
230 below the line, we defined a strip of surface area in each hemisphere that mainly captures the hand area of M1  
231 and S1 (white area in Fig. 2B). We subdivided this area into 50 vertical sections running from anterior to posterior,  
232 allowing us to summarize the result on a one-dimensional profile-view (e.g., Fig 2G,H; Fig. 3E,F). For statistical  
233 analysis only, we combined results by major region (grouping vertical sections together) according to the  
234 cytoarchitectonic probabilistic atlas. We defined the region of interest for the primary motor cortex (M1; BA4),  
235 primary somatosensory cortex (S1; BA 1, 2, and 3), dorsal premotor cortex (PMd; BA 6), and the anterior parietal

lobules (aSPL; BA 5) by selecting the strips that had the highest probability (averaged over all vertices within the strip) as determined by a probabilistic cytoarchitectonic atlas (Fischl et al., 2008) of belonging to their respective BA. The supplementary motor areas (SMA) lay outside of the defined strip of surface area. We therefore defined the SMA ROI by choosing the part of BA6 that was situated in the medial wall.

ROI-based analyses were conducted in the space of the individual data acquisition for each individual participant by determining the voxel that would be projected onto the set of surface nodes associated with each ROI. In this analysis (as well as for surface-based mapping), we excluded voxels with more than 25% of their volume in the grey matter on the opposite side of a sulcus. This avoided cross-contamination of activity measured in M1 and S1, as well as across the pre-central and post-central sulcus. No smoothing of functional activity in the volume was applied. This approach has allowed us in one previous paper to carefully analyze the specialization of subregions of human S1 and M1 (Arbuckle et al., 2022).

### ***Analysis of activation***

We calculated the percent signal change for each condition relative to the baseline activation for each voxel for each functional run and averaged it across runs. For ROI analysis, these values were averaged across all voxels in the native volume space of each participant selected for the respective ROI. For surface-based group maps, individual data were projected onto the group map via the individual surfaces, using all voxels touching the line that connected corresponding nodes on the pial and white-matter surfaces.

Statistical analyses to assess the cortical activity of each sequence type during each phase of preparation or production included a two-sided one-sample t-test vs. zero. For statistical tests on the surface, we used an uncorrected threshold of  $p=0.001$  and controlled the family-wise error by calculating the size of the largest suprathreshold cluster across the entire cortical surface (estimated smoothness of FWHM 7.9 mm) that would be expected by chance ( $p=0.05$ ) using Gaussian field theory as implemented in the *fmrstat* package (Worsley et al., 1996).

### ***Multivariate distance analysis***

To evaluate which brain areas displayed sequence-specific representations, we used the representational similarity analysis (Kriegeskorte & Diedrichsen, 2019). We calculated the cross-validated Mahalanobis distances (Walther et al., 2016) between evoked regional patterns (beta estimates from first-level GLM) of different pairs of conditions, 6 sequences (3 single, 3 multi) x 2 phases (preparation no-go, production). Prior to calculating the distances, beta weights for each condition were spatially pre-whitened (i.e., weighted by the matrix square root of the noise covariance matrix, as estimated from the residuals of the GLM). The noise covariance matrix was slightly regularized towards a diagonal matrix (Ledoit & Wolf, 2003). Multivariate pre-whitening has been shown to increase the reliability of dissimilarity estimates (Walther et al., 2016).

Cross-validation ensures the distance estimates are unbiased, such that if two patterns differ only by measurement noise, the mean of the estimated value would be zero (Diedrichsen et al., 2020). This also means that estimates can sometimes become negative. Therefore, dissimilarities significantly larger than zero indicate that the two patterns are reliably distinct, akin to an above-chance performance in a cross-validated pattern classification analysis.

Multivariate analysis was conducted for ROI and surface analysis. For surface-based maps, we also conducted a searchlight analysis (e.g., Fig 3A). For each surface node, we selected a circular region of 100 voxels (with a maximal radius of 12 mm) and assigned the result to the central node of the searchlight.

### ***Dispersion metric***

To determine whether there were significant differences in the dispersion of the representations for multi- and single-finger sequences during preparation, we first set all negative dissimilarity values to 0. We then normalized the dissimilarities for each sequence type such that all vertices' dissimilarities in the white strip (Fig. 2A) summed up to 1. This defined the weight of each surface vertex. The center-of-gravity (COG) per participant was then the weighted average of the x and y coordinates of these vertices on the flat map. Then, we calculated the dispersion ( $d$ ) around this COG by calculating the squared distance between each vertex and COG and averaging them weighted by  $w_i$ .

$$d = \sum_{i \in \text{vertices}} w_i [(x - COG_x)^2 + (y - COG_y)^2]$$

The difference in dispersion between multi- and single-finger sequences was assessed using a two-sided paired t-test.

### ***Correlation analysis***

To assess the relationship between planning and execution-related activity, we estimated the correlation between them. For estimation, we employed two different approaches. First, we used simple Pearson's correlation. When estimating the correlation between sequence-specific activity patterns, we first removed the mean pattern for the preparation and production phase. We then stacked the three activity patterns into a single vector. The average (across runs) activity patterns for preparation and production were correlated directly. When estimating the correlation between multi vs. single contrasts across preparation and production, we first calculated the difference between activity patterns of 3 multi-finger sequences and the corresponding single-finger movements (i.e., sequence 135351 with 111111, etc.) and then averaged the three maps. The average (across runs) difference maps for preparation and production were then correlated directly. Correlations were calculated separately within each participant. To test for a positive correlation, we performed a two-sided paired t-test against zero.

To obtain an estimate of the correlation, corrected for the level of measurement noise, we used pattern component modelling (PCM, Diedrichsen et al., 2018). The problem with Pearson's correlations estimated on the

noisy data is that they are always smaller than 1, even if the underlying patterns are identical. PCM solves this issue by modelling the noise and true pattern separately and estimating the likelihood of the data given any value of correlation (Diedrichsen et al., 2023). We created 100 correlation models with correlations in the range [0–1] in equal step sizes and assessed the likelihood of the observed data from each participant under each correlation model (Fig. 4C). First, we used the winning model as an estimate of the noise-corrected correlation (maximum-likelihood estimate). To test whether two sets of activity patterns are identical, we compared the likelihood of the best-fitting model within each participant to the likelihood of a competing correlation model ( $r=1$ ), using a two-sided paired Wilcoxon signed-rank test. The choice of the best-fitting model was acquired using a cross-validated approach, estimating the group-winning model from  $n-1$  participants, and determining the log-likelihood of this model for the left-out participant (for whom this model may not be the best one).

### *Analysis of principal components*

To test if the activity patterns for the difference between multi- and single-finger sequences across preparation and production are systematically different in some brain regions, we employed principle component analysis (PCA). The simple contrast between the two difference maps could not answer this question because they have different scales. We obtained the multi vs. single contrast during preparation and production averaged across sequences for all voxels within the region of interest (Fig. 2A, purple area). For each individual, we then conducted a singular value decomposition on the  $2 \times P$  matrix, in which the two rows represented the preparation and production contrasts. The first PC captured the common neural activity shared by processes happening during preparation and production while accounting for the differing degrees of activation in specific voxels. The second PC represented the tendency of each voxel to be relatively more engaged during one process than the other. We ensured that for each participant the positive value on the second PC represented relatively more engagement during the production phase. Lastly, we projected the value for each voxel to the nearest vertex and created a preference map. These maps were then submitted to a surface-based group analysis (see above).

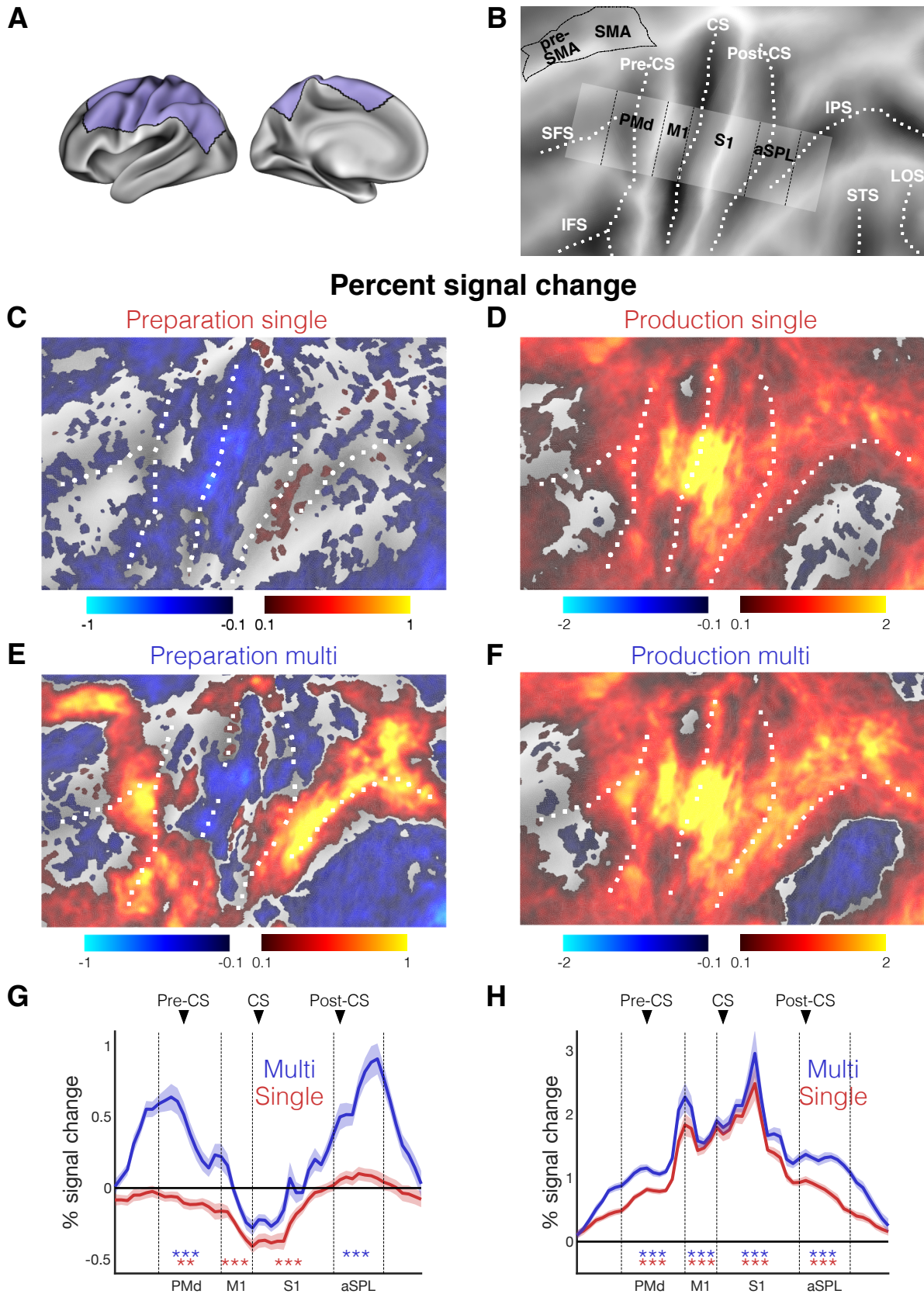
## **Results**

### *Pre-planning of multi-finger sequences activates the first finger in M1 and S1*

First, we asked what processes occur during sequence preparation in the core sensorimotor areas S1 and M1. For single-finger movements (Fig. 2C), BOLD activity in these regions was suppressed relative to rest (Fig. 2G; M1:  $t_{21} = -6.939$ ,  $p = 7.4e-07$ ; S1:  $t_{21} = -5.508$ ,  $p = 1.8e-05$ ). For multi-finger movements (Fig. 2E), we also observed some suppression deep in the central sulcus, however, averaged across the ROI, the activation was not different from the resting baseline (M1:  $t_{21} = -0.692$ ,  $p = 0.496$ ; S1:  $t_{21} = -0.523$ ,  $p = 0.606$ ).

We then used multi-voxel pattern analysis to examine whether the fine-grained pattern of activity in these areas differed between the planned sequences. To this end, we calculated cross-validated Mahalanobis distances

332 (Diedrichsen et al., 2020; Walther et al., 2016) between the activity patterns associated with the 3 sequences.  
333 Systematically positive values of this measure indicate reliable multivariate pattern differences. As previously  
334 reported (Ariani et al., 2022), we found that during the preparation of single-finger movements (Fig. 3A), the core  
335 hand areas of M1 and S1 exhibited finger-specific activity patterns (M1:  $t_{21}=2.343$ ,  $p=0.029$ ; S1:  $t_{21}=3.137$ ,  
336  $p=0.005$ ). Analysis of multi-finger sequences revealed a similar result: although M1 and S1 were not activated  
337 overall, there were significant differences between activity patterns for three sequences (Fig. 3E; M1:  $t_{21}=2.991$ ,  
338  $p=0.007$ ; S1:  $t_{21}=2.829$ ,  $p=0.010$ ).



339

340

341

**Figure 2. Premotor and superior parietal lobule are activated during sequence preparation.** (A) inflated cortical surface of the contralateral (left) hemisphere, highlighting the displayed areas (B-F, purple). (B) Flat

342 representation of the neocortex with major sulci indicated by white dotted lines, and the boundaries of different  
343 regions indicated by black dashed lines. The strip highlighted in white was used for the profiles (G, H) and region-  
344 of-interest definition. **(C)** Group-averaged percent signal change during preparation and **(D)** production of  
345 single-finger sequences. **(E,F)** Same as (C,D) but for multi-finger sequences. **(G)** Profile ROI analysis (see  
346 Materials and methods) of the mean percent signal change ( $\pm$  standard error of the mean [SEM]) during the  
347 preparation and **(H)** production of single-finger (red) and multi-finger sequences (blue). The x-axis corresponds  
348 to Brodmann areas (BA) shown in (B).  $**p < 0.01$ ,  $***p < 0.001$  in a two-sided one-sample t-test vs. zero for  
349 selected ROIs. Vertical black lines mark the approximate boundaries between the BAs (see Methods). Black  
350 triangles point to the approximate location of the main anatomical landmark. Sulci: superior frontal sulcus (SFS),  
351 inferior frontal sulcus (IFS), precentral sulcus (Pre-CS), central sulcus (CS), post central sulcus (Post-CS), intra-  
352 parietal sulcus (IPS), lateral occipital sulcus (LOS), superior temporal sulcus (STS). ROIs: anterior superior-  
353 parietal lobule (aSPL, BA 5), primary somatosensory cortex (S1, BA 3, 1, 2), primary motor cortex (M1), dorsal  
354 premotor cortex (PMd, BA 6), secondary motor area (pre-SMA and SMA, BA 6).

355 What do these activity differences for multi-finger sequences reflect? One possibility is that during  
356 sequence preparation, the first element of the sequences is pre-activated in M1. Because each sequence started  
357 with a different finger, this would cause large differences between the activity patterns without constituting a  
358 sequence representation. This idea predicts that the activity pattern during preparation should correlate with the  
359 activity pattern observed when only the first finger movement is pressed. To test this, we correlated the  
360 preparation activity of 3 multi-finger sequences with the production activity of the corresponding single-finger  
361 sequences (i.e., sequence 135351 with 111111, etc.) after subtracting the mean activity pattern. This analysis  
362 revealed a significant correlation in both M1 (average  $r=0.043$ ,  $t_{21}=2.366$ ,  $p=0.027$ ) and S1 ( $r=0.047$ ,  $t_{21}=2.285$ ,  
363  $p=0.032$ ) but not in PMd ( $t_{21}=-1.227$ ,  $p=0.233$ ) and aSPL ( $t_{21}=-0.242$ ,  $p=0.811$ ) with the values of correlation  
364 being significantly larger in M1/S1 than PMd/aSPL ( $t_{21}=3.068$ ,  $p=0.005$ ). While these correlations are very small,  
365 correlation estimated on noisy data consistently underestimate the true correlation (Diedrichsen et al., 2023). To  
366 account for measurement noise in a principled way, we used Pattern Component Modeling (PCM, see Methods)  
367 to build potential models of the correlation between activity patterns for the preparation of multi-finger sequences  
368 and production of single-finger sequences and evaluate the likelihood of the data given each model. We removed  
369 the average activity pattern common to all sequences from the patterns (separately for multi- and single-finger  
370 sequences), and then correlated the patterns across the two conditions. The group maximum-likelihood estimates  
371 of correlation indicated substantial correspondence with  $r=0.40$  for S1 and  $r=0.34$  for M1. Thus, there is  
372 substantial overlap between the patterns during pre-planning of multi-finger sequences and the patterns during  
373 the execution of the first finger in the sequence.

374 In previous studies, we have found that the activity patterns in M1 and S1 (averaged over preparation and  
375 production phases) can be explained by a temporal summation of the patterns related to the individual finger

presses, with an especially high weight from the first finger in the sequence (Berlot et al., 2021; Yokoi et al., 2018). If this weighting is due to the pre-activation of the first finger during movement preparation, we would predict that the pattern differences between sequences should disappear during the execution phase, as all three involved the same three fingers (albeit in a different order). Indeed, the pattern differences were significantly attenuated during the production phase (Fig. 3D, planning vs. execution in M1:  $t_{21}=2.123$ ,  $p=0.0458$ , and S1:  $t_{21}=2.305$ ,  $p=0.0345$ ), with a small pattern difference remaining only in M1 ( $t_{21}=2.814$ ,  $p=0.0104$ ).

In sum, these results are consistent with the idea that the first finger in a sequence is pre-activated during the preparation phase and that after production starts, the activity pattern in M1 and S1 are determined by a temporal summation of the patterns related to the individual finger presses (Yokoi et al., 2018).

### ***Pre- and online planning engage a highly overlapping set of cortical areas***

If the activity patterns in the M1 and S1 are related to the individual finger presses, then continuous input from higher-level regions that retain a representation of the entire sequence is required to move reliably from finger to finger. We refer to this process as planning, whether it occurs before (pre-planning) or after movement onset (online planning; Ariani & Diedrichsen, 2019; Ariani et al., 2021). Here investigate whether pre- and online planning engage exactly the same, or different sets of cortical areas. Given that the number, speed, and force of the finger presses were closely matched across single and multi-finger movements (Table 1), we assumed that both conditions involve similar execution-related processes. Therefore, the difference between the production of single-finger and multi-finger sequences should mostly reflect activity related to online planning. If pre-planning and online planning involve the exact same cortical areas, then this difference should be similar to the difference between single-finger and multi-finger movement during preparation (reflecting the need for increased pre-planning).

	Single-finger	Multi-finger	Difference
ET [ms]	1450 ± 58	1370 ± 70	$t_{21}=1.815$ , $p=0.083$
Force [N]	1.7 ± 0.1	1.8 ± 0.1	$t_{21}=1.423$ , $p=0.169$

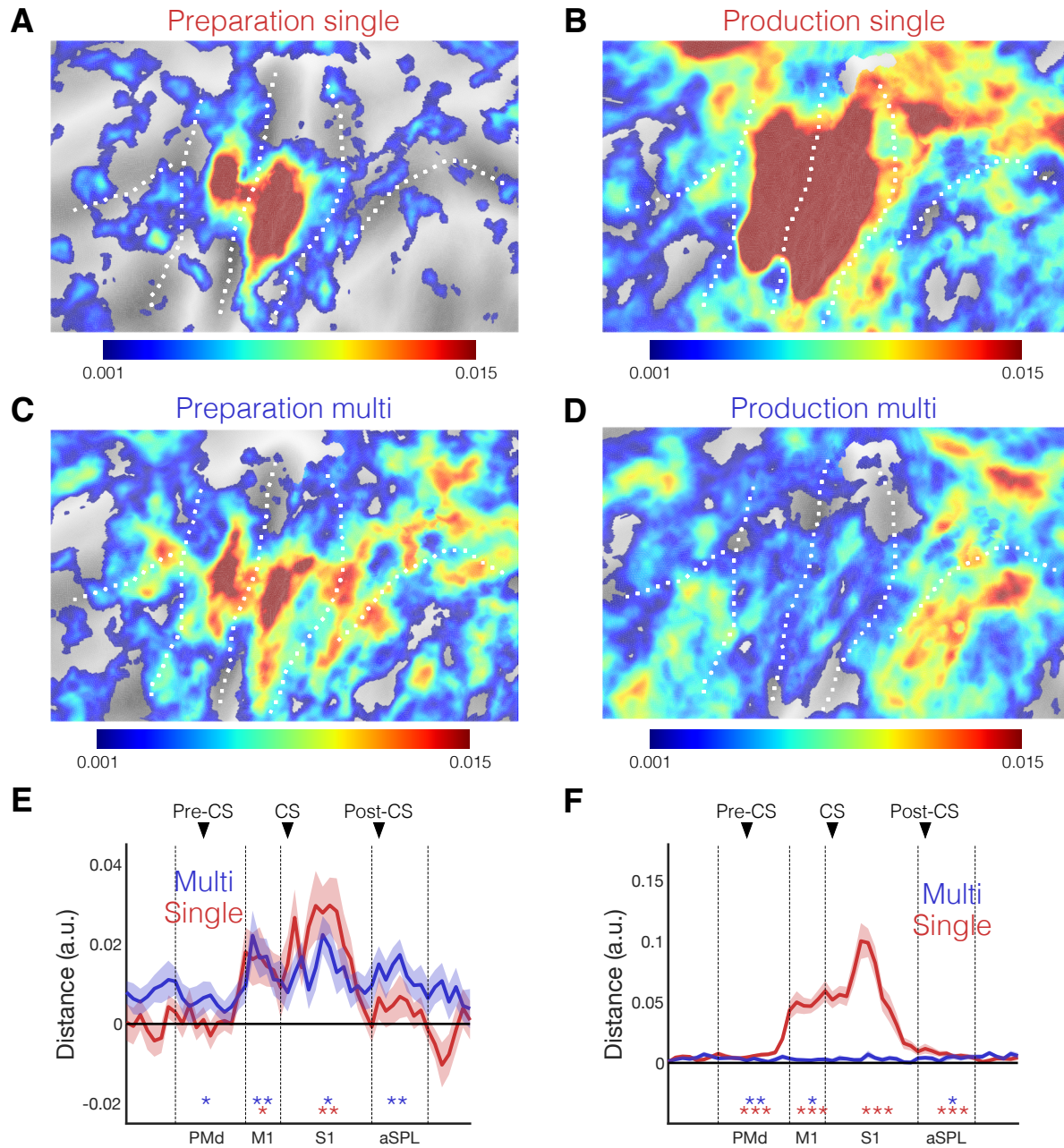
Table 1. Average execution time (ET, i.e., time needed to complete a sequence) and average peak force for single-finger and multi-finger sequences across participants. A two-sided paired t-test for a difference between conditions is reported in the last column.

In contrast to single-finger movements (Fig. 2C), preparation of multi-finger sequences (Fig. 2E) strongly activated the dorsal premotor cortex (Fig. 2G; PMd,  $t_{21}=5.125$ ,  $p=4.4e-05$ ), the supplementary motor areas (SMA/pre-SMA,  $t_{21}=4.016$ ,  $p=2.3e-04$ ) and the anterior part of the superior parietal lobule (aSPL,  $t_{21}=7.482$ ,  $p=2.3e-07$ ). Thus, the demands of planning multiple different finger movements evoked significant brain activation in premotor and parietal areas.

405 During the production, we found widespread activity in both primary sensorimotor, parietal, and pre-  
406 motor areas for both sequence types (Fig. 2D, F). The contrast between these two conditions revealed higher  
407 activity for multi-finger over single-finger sequences in PMd (Fig. 2H, 4B;  $t_{21}=6.022$ ,  $p=5.6e-6$ ) and aSPL  
408 ( $t_{21}=8.264$ ,  $p=4.8e-08$ ). In contrast, in caudal M1 and rostral S1 the same two conditions elicited very similar  
409 activity levels, consistent with the idea that the basic motor requirements were well matched between single- and  
410 multi-finger sequences.

411 Importantly, the spatial distribution of multi vs. single contrast during production was very similar to multi  
412 vs. single contrast during preparation (Fig. 4A, B). When we correlated the unsmoothed voxel-wise activity maps  
413 within each participant, we found a highly significant correlation between the brain activity patterns under these  
414 two conditions ( $r=0.12$ ,  $t_{21}=10.796$ ,  $p=4.9e-10$ ). Thus, pre- and online planning activated overlapping cortical  
415 areas.

## Crossnobis distance



416

417

418

419

420

421

422

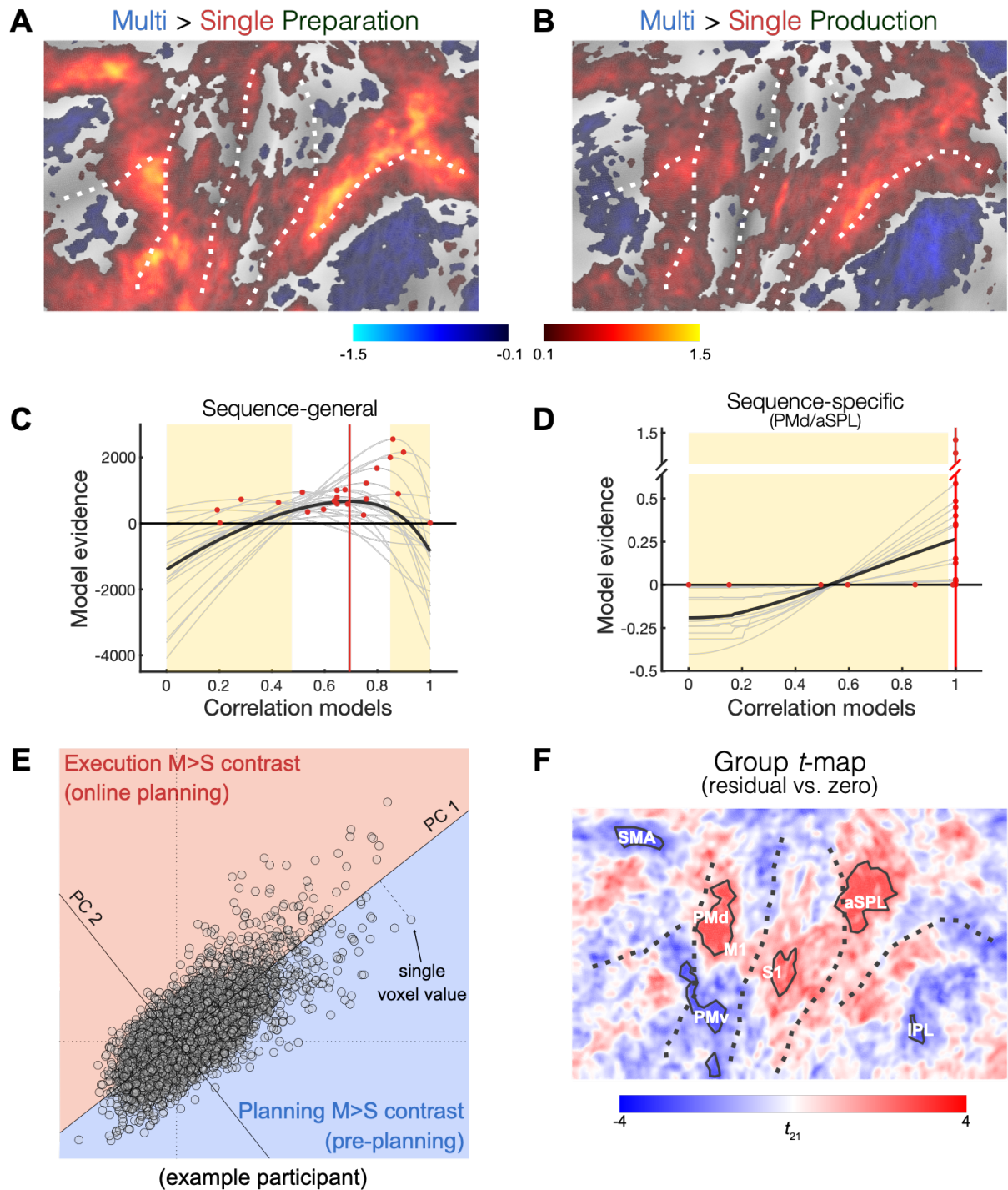
423

**Figure 3. Sequence representations during preparation and production phases.** (A) Group-averaged multivariate searchlight map of the crossnobis distance between the preparation and (B) production of the three single-finger. (C) Same as A but for mean crossnobis distance between the preparation and (D) production of three multi-finger sequences. (E) Profile ROI analysis of the mean crossnobis distance (±SEM) during the preparation of single-finger (light red line) and multi-finger (light blue) sequences. (F) Same as E but for the production of single-finger (dark blue) and multi-finger (dark red) sequences. \* $p < 0.05$ , \*\* $p < 0.01$ , \*\*\* $p < 0.001$  in a two-sided one-sample  $t$ -test vs. zero for selected ROIs.

## 424 ***Preferential activation for planning before and during movement***

425 The strong overlap between the activity maps for pre- and online planning, however, does not tell us whether the  
426 two maps were identical (in other words, pre- and online planning activated - within each participant - exactly the  
427 same voxels) or whether there were true differences between the maps. This is because measurement noise will  
428 lead to an observed correlation smaller than 1, even if two maps are identical (Diedrichsen et al., 2023). Again,  
429 we applied PCM to model the correlation between multi-single contrast activity patterns in both preparation and  
430 production, followed by an assessment of data likelihood for each model (see Fig. 4C). The group maximum-  
431 likelihood estimate of correlation was  $r=0.65$  with strong evidence that the patterns were not identical (against 1-  
432 corr model:  $z = 3.815$ ,  $p=0.0001$ ).

433 Therefore, we asked whether there were systematic differences across participants, which would indicate  
434 that some areas have a preference toward either pre- or online planning. Because the contrast during pre-planning  
435 was generally larger than during execution, we could not simply subtract the two difference maps. Instead, we  
436 plotted the multi-single difference for each voxel during preparation (Fig. 4E, x-axis) against the difference during  
437 production (y-axis). We then estimated the average relationship between the two contrasts using Principal  
438 Component Analysis (PCA) within each participant. The first principal component (PC1) captured the tendency  
439 of voxels to be similarly responsive for pre- or online planning. The loading on the second principal component  
440 captured the deviation from this lawful relationship, with positive values indicating relatively more activity during  
441 online planning and negative values more activity during pre-planning. By mapping the voxel preferences back  
442 to the surface, we created an average preference map across participants within our window of interest (Fig. 4F).  
443 This map revealed that clusters (solid outlines in Fig. 4F) in PMd ( $p=5.9e-07$ , corrected for multiple comparisons,  
444 see Methods), M1/S1 ( $p=8.8e-06$ ), and aSPL ( $p=5.9e-07$ ) were more active during online planning, while clusters  
445 in SMA ( $p=3.1e-06$ ), the ventral premotor cortex (PMv,  $p=7.2e-07$  and  $p=0.0096$ ), and the inferior parietal lobule  
446 (IPL,  $p=0.0492$ ) were relatively more active during pre-planning (Fig. 4F). This set of results indicates that pre-  
447 planning and online planning of movement sequences preferentially activated slightly different sets of cortical  
448 areas.



450  
 451 **Figure 4. Activation maps for pre- and online planning are highly, but not perfectly, correlated.** (A) The  
 452 difference in evoked activation between multi-finger and single-finger sequences during the preparation and (B)  
 453 production. (C) PCM evaluation of models assuming a correlation between the sequence-general activity patterns  
 454 shown in A and B of 0 to 1. The group average (black line) and individual curves (thin gray lines) express the  
 455 difference from the log-likelihood from the mean value (i.e., zero on the y-axis). Red dots indicate the best-fitting  
 456 correlation model for each participant and the red solid line cross-validated best-fitting model across all  
 457 participants. Yellow-shaded area indicates models that perform significantly worse than the best-fitting

458 correlation model ( $p < 0.05$ ). **(D)** Similar to (C), but for the correlation between sequence-specific activity  
459 patterns evoked during preparation and production of multi-finger sequences in PMd and aSPL. For each  
460 participant, we averaged the curve corresponding to each of the two areas. **(E)** Voxel-wise values of the  
461 preparation multi-single contrast, plotted against the voxel-wise values of the production multi-single contrast.  
462 Two principal components (PCs) of the data are shown. Voxels in the red area (positive PC2) show a preference  
463 for online planning, whereas voxels in the blue area (negative PC2) show for pre-planning. An example of a  
464 single participant is shown. **(F)** Group  $t$ -value for the second PC projected on the flat map. Areas with black solid  
465 outlines represent significant clusters. Note that for this surface-based (rather than ROI-based) analysis, there is  
466 no strict correspondence between the clusters on the map and our pre-defined ROIs. The labels next to the  
467 significant clusters correspond to the more closely matching ROI.

### 468 ***PMd and SPL maintain sequence-specific representations both during preparation and production***

469 If the increased activation for multi-finger sequences in PMd and SPL (Fig. 4A-B) was related to pre-planning  
470 and online planning, then these areas should exhibit sequence-specific representations during both the preparation  
471 and production phases.

472 Indeed, for the preparation phase multivariate analysis (Fig. 3C) revealed that both areas showed  
473 sequence-specific representations of multi-finger sequences. We found significant pattern differences in PMd  
474 (Fig. 3E,  $t_{21} = 2.266$ ,  $p=0.034$ ) and aSPL ( $t_{21}=3.491$ ,  $p=0.002$ ). In contrast to the preparation of single-finger  
475 movements (Fig. 3A), the representations of multi-finger sequences appeared to be more widespread on the  
476 cortical sheet. To quantify this observation, we calculated a spatial dispersion metric, which reflects the spatial  
477 variance of pattern dissimilarities (see Methods). This analysis confirmed that the planning of multi-finger  
478 sequences was associated with a more widespread representation across the sensory-motor network compared  
479 with single-finger sequences ( $t_{21}=3.542$ ,  $p=0.002$ ). Therefore, premotor and parietal areas were not only more  
480 active during the preparation of multi- than single-finger sequences (Fig. 4A), but also represented the identity of  
481 the sequence.

482 Importantly, we also found that these representations were maintained during the execution phase (Fig.  
483 3D, PMd:  $t_{21}=3.221$ ,  $p=0.004$ ; aSPL:  $t_{21}=2.490$ ,  $p=0.021$ ). When comparing the multivariate distances between  
484 preparation (Fig. 3C) and execution (Fig. 3D) we found a strong reduction in M1 ( $t_{21}=2.123$ ,  $p=0.045$ ) and S1  
485 ( $t_{21}=2.305$ ,  $p=0.0314$ ). In contrast, the pattern differences in PMd and aSPL did not attenuate from the preparation  
486 to the execution phase (PMd:  $t_{21}=0.271$ ,  $p=0.7889$ , and aSPL:  $t_{21}=1.895$ ,  $p=0.0719$ ). Note that the multivariate  
487 distances reported in Fig. 3 are measured with noise, so the small-scale differences that can be observed between  
488 Fig. 3C and Fig. 3D should not be overinterpreted. When conducting a map-wise comparison, none of the subtle  
489 differences are significant after controlling for multiple comparisons. We therefore chose a ROI approach to

490 increase our statistical power. These results are consistent with the idea that premotor and parietal areas are  
491 involved in the planning of movement sequences both before and during sequence production.

492 Finally, we asked whether the sequence-specific representations in these areas remained stable or whether  
493 they changed dynamically from preparation to production. To address this question, we again used PCM. We  
494 removed the average activity pattern common to all multi-finger sequences from the patterns (separately for  
495 preparation and production phase), and then correlated these sequence-specific pattern differences between  
496 sequences across the two phases. Figure 4D shows the likelihood curves for different correlation models averaged  
497 across PMd and aSPL. The small signal-to-noise for relatively subtle differences between multi-finger sequences  
498 resulted in small model evidence for almost all participants. The cross-validated group-winning model predicted  
499 that sequence-specific activity patterns were perfectly correlated with strong evidence that patterns were not  
500 uncorrelated (against 0-corr model: PMd:  $z = 2.646$ ,  $p=0.008$ ; aSPL:  $z = 2.873$ ,  $p=0.004$ ). These results suggest  
501 that sequence-specific representations remain stable across pre-planning and execution.

## 502 **Discussion (1500 max)**

503 We used 7T fMRI and multivariate analyses to investigate the role of human cortical areas in the preparation of  
504 movement sequences, separating processes that occur before and during movement production. We found that  
505 primary sensorimotor cortices (M1, S1) showed activity patterns resembling the first movement in the sequence  
506 during preparation, and of a temporal summation of individual movements during production. In contrast,  
507 secondary sensorimotor areas (PMd, SMA, SPL) were more activated during both pre- and online planning of  
508 motor sequences. These regions also maintained a stable representation of the sequence across preparation and  
509 production phases.

510 In previous fMRI studies, we found that the activity patterns in M1 and S1 during sequence production  
511 can be explained by the linear combination of the patterns associated with the individual movements (Berlot et  
512 al., 2021; Yokoi & Diedrichsen, 2019). The pattern for the first finger in the sequence contributed substantially  
513 more to the overall pattern (average over preparation and execution) than all the subsequent fingers (Yokoi et al.,  
514 2018). Our results now provide evidence that this *'first finger effect'* was caused by the pre-activation of the first  
515 sequence element during preparation rather than by the transition from planning to execution state space  
516 (Kaufman et al., 2016; Yokoi et al., 2018): the pre-planning of a multi-finger sequence activated a pattern similar  
517 to that observed during the execution of the first movement in that sequence.

518 In a study using sequences of object-directed reach-to-grasp movements, Gallivan et al. (2016) found that  
519 the activity patterns in M1 were also slightly different between two sequences that started with the same  
520 movement but differed in the second movement. This suggests that, not only the first, but possibly also the second  
521 movement may be reflected in M1 preparatory activity patterns. This observation would be consistent with the  
522 “competitive queuing” hypothesis (Averbeck et al., 2002), the idea that the first movement in a sequence being

523 most, the second less, and subsequent movements even less activated (Kornysheva et al., 2019). However,  
524 because the first reach-to-grasp movement was always the same across conditions, it was unclear whether these  
525 findings would generalize to longer and more complex sequences where every sequence element is different and  
526 needs to be planned anew from trial to trial.

527 After sequence production began, the pattern differences in M1 and S1 between the 3 multi-finger  
528 sequences were strongly attenuated. This is likely due to the fact the pattern corresponding to the single-finger  
529 movements were sequentially activated. Due to the low temporal resolution of fMRI, these patterns combined  
530 additively, such that the three multi-finger sequences (which were matched in terms of the involved fingers)  
531 elicited overall similar activity pattern when we isolated the activity during the production phase.

532 These results also suggest that the production of the sequence cannot be maintained autonomously by  
533 primary motor areas, but that it depends on input from secondary motor areas (Russo et al., 2020; Tanji & Shima,  
534 1994; Yokoi & Diedrichsen, 2019). Consistent with this idea, we found that PMd, SMA, and SPL (but not caudal  
535 M1 and rostral S1) were more activated during the preparation and production of multi-finger as compared to  
536 single-finger movements. We also found sequence-specific activity patterns in these areas, which were correlated  
537 across preparation and production phases. This suggests that premotor and parietal areas maintained a stable  
538 representation of the sequence throughout, likely to drive the next movements in M1.

539 As shown in recent behavioral studies (Ariani & Diedrichsen, 2019; Ariani et al., 2021; Kashefi et al.,  
540 2023), even relatively short 5-item sequences cannot be fully pre-planned. Instead, planning of remaining items  
541 needs to continue throughout sequence production. To determine if the same areas are involved in the pre- and  
542 online planning, we contrasted the univariate multi-finger to single-finger activity maps. As basic execution  
543 processes were matched, we interpreted these contrasts as reflecting the increased need for planning. We found  
544 that the contrast maps were highly correlated across preparation and production phases (Fig. 4C), indicating that  
545 pre-planning and online planning activated similar regions. Within two of these regions, the PMd and aSPL, we  
546 also found that the sequence-specific activity patterns were highly correlated across these preparation and  
547 production (Fig. 4D), suggesting that the sequence-specific representations remained stable. Together these two  
548 findings are evidence that the processes involved in online planning are similar to those involved in pre-planning.

549 Despite considerable overlap in brain activation between pre- and online planning (Fig. 3A,B), however,  
550 further analysis revealed small but systematic differences in the involvement of different brain areas: PMd, S1,  
551 and SPL tended to be more active during online planning, and SMA and ventral premotor cortex (PMv) more  
552 during pre-planning. This indicates that the two processes are not exactly identical. One possible explanation  
553 could be the differential engagement of brain areas in memory encoding and memory retrieval processes that, as  
554 part of planning processes, happened during preparation and production, respectively. The exact nature of these  
555 differences, however, remains to be tested in future studies.

Our results offer testable predictions for future neurophysiological recordings in sensorimotor areas of non-human primates. They predict that M1 shows fast dynamics related to each individual movement, with linear superposition of subsequent movements (Zimnik & Churchland, 2021). Additionally, they predict the presence of sequence-specific representation in premotor and superior parietal areas both during preparation and production. The observed consistency of these representations during preparation and production suggests that these representations have slow dynamics and change very little from preparation to production. However, it is also possible that these patterns are stable at a voxel level—i.e., pre- and online planning activate the same cortical columns—but show faster dynamics at the single neuron level. Studying these representations at a neuronal level at high temporal resolution will provide additional insight into how the motor system solves the fundamental problem of serial order in behavior (Lashley, 1951).

## References

- Arbuckle, S. A., Andrew Pruszynski, J., & Diedrichsen, J. (2022). Mapping the Integration of Sensory Information across Fingers in Human Sensorimotor Cortex. *The Journal of Neuroscience: The Official Journal of the Society for Neuroscience*, *42*(26), 5173–5185.
- Ariani, G., & Diedrichsen, J. (2019). Sequence learning is driven by improvements in motor planning. *Journal of Neurophysiology*, *121*(6), 2088–2100.
- Ariani, G., Kordjazi, N., Pruszynski, J. A., & Diedrichsen, J. (2021). The Planning Horizon for Movement Sequences. *ENeuro*, *8*(2). <https://doi.org/10.1523/ENEURO.0085-21.2021>
- Ariani, G., Oosterhof, N. N., & Lingnau, A. (2018). Time-resolved decoding of planned delayed and immediate prehension movements. *Cortex; a Journal Devoted to the Study of the Nervous System and Behavior*, *99*, 330–345.
- Ariani, G., Pruszynski, J. A., & Diedrichsen, J. (2022). Motor planning brings human primary somatosensory cortex into action-specific preparatory states. *ELife*, *11*. <https://doi.org/10.7554/eLife.69517>
- Averbeck, B. B., Chafee, M. V., Crowe, D. A., & Georgopoulos, A. P. (2002). Parallel processing of serial movements in prefrontal cortex. *Proceedings of the National Academy of Sciences of the United States of America*, *99*(20), 13172–13177.
- Berlot, E., Popp, N. J., & Diedrichsen, J. (2020). A critical re-evaluation of fMRI signatures of motor sequence learning. *ELife*, *9*, e55241.
- Berlot, E., Popp, N. J., Grafton, S. T., & Diedrichsen, J. (2021). Combining Repetition Suppression and Pattern Analysis Provides New Insights into the Role of M1 and Parietal Areas in Skilled Sequential Actions. *The Journal of Neuroscience: The Official Journal of the Society for Neuroscience*, *41*(36), 7649–7661.

- 588 Berlot, E., Prichard, G., O'Reilly, J., Ejaz, N., & Diedrichsen, J. (2019). Ipsilateral finger representations in the  
589 sensorimotor cortex are driven by active movement processes, not passive sensory input. *Journal of*  
590 *Neurophysiology*, *121*(2), 418–426.
- 591 Dale, A. M., Fischl, B., & Sereno, M. I. (1999). Cortical surface-based analysis. I. Segmentation and surface  
592 reconstruction. *NeuroImage*, *9*(2), 179–194.
- 593 Diedrichsen, J., Shahbazi, M., Ariani, G., & Berlot, E. (2023). Estimating correlations between noisy activity  
594 patterns. A tricky problem with a generative solution. *Diedrichsenlab*.  
595 [https://www.diedrichsenlab.org/BrainDataScience/noisy\\_correlation/index.htm](https://www.diedrichsenlab.org/BrainDataScience/noisy_correlation/index.htm)
- 596 Diedrichsen, Jörn, Berlot, E., Mur, M., Schütt, H. H., Shahbazi, M., & Kriegeskorte, N. (2020). Comparing  
597 representational geometries using whitened unbiased-distance-matrix similarity. In *arXiv [stat.AP]*.  
598 arXiv. <http://arxiv.org/abs/2007.02789>
- 599 Diedrichsen, Jörn, Wiestler, T., & Krakauer, J. W. (2013). Two distinct ipsilateral cortical representations for  
600 individuated finger movements. *Cerebral Cortex*, *23*(6), 1362–1377.
- 601 Diedrichsen, Jörn, Yokoi, A., & Arbuckle, S. A. (2018). Pattern component modeling: A flexible approach for  
602 understanding the representational structure of brain activity patterns. *NeuroImage*, *180*, 119–133.
- 603 Eickhoff, S. B., Grefkes, C., Zilles, K., & Fink, G. R. (2007). The somatotopic organization of cytoarchitectonic  
604 areas on the human parietal operculum. *Cerebral Cortex (New York, N.Y.: 1991)*, *17*(8), 1800–1811.
- 605 Fischl, B., Sereno, M. I., Tootell, R. B., & Dale, A. M. (1999). High-resolution intersubject averaging and a  
606 coordinate system for the cortical surface. *Human Brain Mapping*, *8*(4), 272–284.
- 607 Fischl, Bruce, Rajendran, N., Busa, E., Augustinack, J., Hinds, O., Yeo, B. T. T., Mohlberg, H., Amunts, K., &  
608 Zilles, K. (2008). Cortical folding patterns and predicting cytoarchitecture. *Cerebral Cortex*, *18*(8), 1973–  
609 1980.
- 610 Gallivan, J. P., Johnsrude, I. S., & Flanagan, J. R. (2016). Planning Ahead: Object-Directed Sequential Actions  
611 Decoded from Human Frontoparietal and Occipitotemporal Networks. *Cerebral Cortex*, *26*(2), 708–730.
- 612 Hutton, C., Bork, A., Josephs, O., Deichmann, R., Ashburner, J., & Turner, R. (2002). Image distortion correction  
613 in fMRI: A quantitative evaluation. *NeuroImage*, *16*(1), 217–240.
- 614 Kashefi, M., Reschechtko, S., Ariani, G., Shahbazi, M., Die-drichsen, J., & Andrew Pruszynski, J. (2023).  
615 Interaction of multiple future movement plans in sequential reaching. In *bioRxiv* (p. 2023.05.24.542099).  
616 <https://doi.org/10.1101/2023.05.24.542099>
- 617 Kaufman, M. T., Seely, J. S., Sussillo, D., Ryu, S. I., Shenoy, K. V., & Churchland, M. M. (2016). The largest  
618 response component in the motor cortex reflects movement timing but not movement type. *ENeuro*, *3*(4),  
619 ENEURO.0085-16.2016.
- 620 Kornysheva, K., Bush, D., Meyer, S. S., Sadnicka, A., Barnes, G., & Burgess, N. (2019). Neural Competitive  
621 Queuing of Ordinal Structure Underlies Skilled Sequential Action. *Neuron*, *101*(6), 1166-1180.e3.

- 622 Kriegeskorte, N., & Diedrichsen, J. (2019). Peeling the Onion of Brain Representations. *Annual Review of*  
623 *Neuroscience*, 42, 407–432.
- 624 Lashley, K. S. (1951). *The Problem of Serial Order in Behavior*.
- 625 Ledoit, O., & Wolf, M. N. (2003). Honey, I shrunk the sample covariance matrix. *SSRN Electronic Journal*.  
626 <https://doi.org/10.2139/ssrn.433840>
- 627 Marcus, D. S., Harwell, J., Olsen, T., Hodge, M., Glasser, M. F., Prior, F., Jenkinson, M., Laumann, T., Curtiss,  
628 S. W., & Van Essen, D. C. (2011). Informatics and data mining tools and strategies for the human  
629 connectome project. *Frontiers in Neuroinformatics*, 5, 4.
- 630 Russo, A. A., Khajeh, R., Bittner, S. R., Perkins, S. M., Cunningham, J. P., Abbott, L. F., & Churchland, M. M.  
631 (2020). Neural Trajectories in the Supplementary Motor Area and Motor Cortex Exhibit Distinct  
632 Geometries, Compatible with Different Classes of Computation. *Neuron*, 107(4), 745-758.e6.
- 633 Shima, K., Isoda, M., Mushiake, H., & Tanji, J. (2006). Categorization of behavioural sequences in the prefrontal  
634 cortex. *Nature*, 445(7125), 315–318.
- 635 Tanji, J., & Shima, K. (1994). Role for supplementary motor area cells in planning several movements ahead.  
636 *Nature*, 371(6496), 413–416.
- 637 Van Essen, D. C., Glasser, M. F., Dierker, D. L., Harwell, J., & Coalson, T. (2012). Parcellations and hemispheric  
638 asymmetries of human cerebral cortex analyzed on surface-based atlases. *Cerebral Cortex*, 22(10), 2241–  
639 2262.
- 640 Walther, A., Nili, H., Ejaz, N., Alink, A., Kriegeskorte, N., & Diedrichsen, J. (2016). Reliability of dissimilarity  
641 measures for multi-voxel pattern analysis. *NeuroImage*, 137, 188–200.
- 642 Worsley, K. J., Marrett, S., Neelin, P., Vandal, A. C., Friston, K. J., & Evans, A. C. (1996). A unified statistical  
643 approach for determining significant signals in images of cerebral activation. *Human Brain Mapping*,  
644 4(1), 58–73.
- 645 Yokoi, A., Arbuckle, S. A., & Diedrichsen, J. (2018). The Role of Human Primary Motor Cortex in the Production  
646 of Skilled Finger Sequences. *The Journal of Neuroscience: The Official Journal of the Society for*  
647 *Neuroscience*, 38(6), 1430–1442.
- 648 Yokoi, A., & Diedrichsen, J. (2019). Neural Organization of Hierarchical Motor Sequence Representations in the  
649 Human Neocortex. *Neuron*, 103(6), 1178-1190.e7.
- 650 Yousry, T. A., Schmid, U. D., Alkadhi, H., Schmidt, D., Peraud, A., Buettner, A., & Winkler, P. (1997).  
651 Localization of the motor hand area to a knob on the precentral gyrus. A new landmark. *Brain: A Journal*  
652 *of Neurology*, 120 ( Pt 1), 141–157.
- 653 Zimnik, A. J., & Churchland, M. M. (2021). Independent generation of sequence elements by motor cortex.  
654 *Nature Neuroscience*, 24(3), 412–424.